Research Article | Vol. 10, No. 12 / 1 December 2019 / Biomedical Optics Express 6043
Biomedical Optics EXPRESS

Spectral indexes obtained by implementation of the fractional Fourier and Hermite transform for the diagnosis of malignant melanoma

ESBANYELY GARZA-FLORES,[1] ESPERANZA GUERRA-ROSAS,[2,3] AND JOSUÉ ÁLVAREZ-BORREGO[3,*]

[1] *SolexVintel, Camino Real de Tetelpan No. 180, Colonia Tetelpan, Alcaldía Álvaro Obregón, Ciudad de México, C. P. 01790, Mexico*
[2] *CETYS University, Camino a Microondas Trinidad s/n. Km. 1, Moderna Oeste, 22860, Ensenada, B. C., Mexico*
[3] *CICESE, División de Física Aplicada, Departamento de Óptica, Carretera Ensenada-Tijuana, No. 3918, Fraccionamiento Zona Playitas, Ensenada, B.C., C.P. 22860, Mexico*
[*] *josue@cicese.mx*

Abstract: Many people suffer from different skin diseases, which can be diverse and varied. Most skin diseases cause disorders in the skin, such as changes in color, texture, and appearance manifesting in spots, swelling, scaling, ulcers, etc. One of the diseases that represents a serious health problem is skin cancer. The most dangerous skin cancer is malignant melanoma, which can cause death if not detected early. Therefore, development of new and accurate diagnosis methodologies to increase the chance of early detection is important. In this work, an analysis to discriminate between malignant melanoma and three types of benign skin lesions–melanocytic nevus, dermatofibroma, and seborrheic keratosis–is realized by calculating spectral indexes based on the real and imaginary parts of a fractional nonlinear filter obtained by affecting the modulus of the fractional Fourier transform by an exponent k. The fractional spectral indexes were calculated by working with selected sub-images obtained by dividing the input image. Also, a variation was implemented when the Hermite transform is used to calculate the fractional nonlinear filter. Discrimination between malignant melanoma and benign skin lesions was achieved with a 99.7% confidence level.

1. Introduction

The identification and classification of skin lesions are essential for the diagnosis of any disease. Skin lesions are alterations in the surface of the skin; which can be caused by pathological change. Many conditions affect humans, and skin cancer is one of them, which is an abnormal growth of skin cells. Some lesions or tumors on the skin may be non-cancerous. Melanocytic nevus, dermatofibroma, and seborrheic keratosis are some of the benign skin lesions. Melanocytic nevus is a benign skin condition characterized by an abnormally dark spot, can be flat or raised; it is composed of pigment-producing cells [1,2]. A person may have congenital or acquired melanocytic nevus. Melanocytic nevus is benign tumors and can appear anywhere on the body; its color varies with time and may be lighter or darker. However, large ones may increase the risk of developing melanoma. Dermatofibroma is a common benign tumor or lesion of oval or round shape and grows slowly with a yellowish or brownish-gray color; its consistency is hard. This tumor can measure from a few millimeters to 2 centimeters, and it occurs more frequently in women. Dermatofibroma is a benign tumor without the risk of becoming malignant. Usually, its diagnosis is by ocular inspection. It presents some characteristics similar to melanoma, so its detection may be confusing [2]. Seborrheic Keratosis is another benign tumor that occurs on the skin, has a light to dark brown color, and slightly elevated with a warty surface and sometimes

#378267 https://doi.org/10.1364/BOE.10.006043
Journal © 2019 Received 18 Sep 2019; revised 22 Oct 2019; accepted 23 Oct 2019; published 4 Nov 2019

Biomedical Optics EXPRESS

with a slight flake. Its diameters vary from 1 millimeter to 4 centimeters; it is usually located in the head or trunk. It occurs more often in areas of the body exposed to the sun. It appears more frequently in adults [3]. Seborrheic Keratosis is soft and greasy to the touch, appears on the healthy skin. Rarely, there are cases of melanoma that arise within or that are adjacent to seborrheic keratosis. Skin cancer is a malignant disease that is generated by division and uncontrolled grown of the cells that make it up. It can invade tissues, healthy structures, and even organs from a distance. There are three main types of skin cancer: basal cell carcinoma, squamous cell carcinoma, and melanoma. From all the types of skin cancer, malignant melanoma is the least common even though it is the most dangerous because of the ability to take place anywhere on the skin [4]. It can spread to other organs in the body (metastasis). If it is not detected early it can cause death, but it is almost curable in its early stages [5]. It can have a variety of colors that include white, brown, black-blue, red, or even light gray.

The principal risk factors related to skin cancer are exposure to the sun, skin color, climate, age, and genetic predisposition. For the diagnosis of skin diseases, one of the steep is to classify skin lesions for preventing the spread of cancer, by making its early detection increases the possibility of cure cancer. Currently, the interest in the development of automated techniques that allow analyzing dermatological images has increased. Visual inspection of the skin for new spots that change size, shape, and color, is the most common way to detect malignant melanoma, and early detection can avoid death [6]. Therefore, the search for better diagnostic methods has been a concern for dermatologists.

The image analysis of skin spots has allowed an essential advance in the diagnosis and treatment of diseases. Dermofit Image Library contains a set of images with various conditions or skin lesions; these images are of high quality and have been confirmed by biopsies and histopathology examination. Different workgroups that belong to universities, hospitals, and departments of dermatology collaborate for Dermofit Image Library, which is used for the analysis of skin lesions [7,8]. In recent years' digital image processing has been used as an alternative for developing methods in this area to provide an accurate and automatic diagnosis with the advantage of being noninvasive for the patient [9]. Various studies for malignant melanoma have been done. In 2011 Gola *et al*. [10] developed an algorithm based on obtaining the shape of the skin lesion to extract features of interest. A similar method was proposed by Rahman and Bhattacharya [11] to discriminate from malignant melanoma, benign lesions, and dysplastic nevi. They used classifiers such as support vector machine (SVM), k-nearest neighbors (K-NNs), and Gaussian maximum likelihood (G-ML), to detect the morphology of the lesion in grayscale applying segmentation. Then color features are extracted and used to train the classifiers. The highest precision obtained was 72.5%. Abdul Jaleel *et al.* [12] proposed a methodology based on artificial neuronal networks to classify malignant melanoma from other skin diseases. Noise from the images was removed first by a preprocessing stage; then, it is smoothed by a median filter. In a later stage, the image is segmented and binarized by applying a threshold, and a 2D wavelet transform is applied to the segmented image to extract features like the mean, standard deviation, absolute mean, L1 norm, and L2 norm and used to train the network. Betta *et al.* [13] described a method for detecting the atypical pigmented network. In this methodology, a combination of structural and spectral techniques was used. The texture defined by local discontinuities like lines and points is identified by the fundamental method. Fourier analysis is used for the spectral approach to obtain the spatial period of texture; in this way, a "regions with a network" mask is created. Recently Guerra-Rosas and Álvarez-Borrego [14] developed a methodology for the diagnosis of skin cancer on images of dermatological spots by using sub-images selected from a segmented image to calculate four different spectral indexes obtained from the real and imaginary parts of various filters. Also, Guerra-Rosas *et al.* [15] developed a method for the detection of malignant melanoma in tissues based on signatures via spectral densities.

Biomedical Optics EXPRESS

In this work, discrimination from malignant melanoma and three types of benign skin lesions are performed by calculating four spectral indexes based on the real and imaginary parts of a nonlinear filter obtained from the fractional Fourier transform (FrFT) of an input image. The ordinary Fourier transform is a particular case of fractional Fourier transform; it is also a valuable tool for signal processing. A variation when the nonlinear filter is obtained by calculating the FrFT of the Hermite transform (HT) of the input image was also performed.

The rest of the paper is organized as follows. In section 2, a description of the images used and the segmentation process is explained. In part 3, the definition of the FrFT is presented. Section 4 defines a fractional nonlinear filter. The definition of the HT is presented in part 5. Section 6 describes the discrimination methodology used to analyze skin lesions, with a variation implementing the HT. In section 7, computer analysis and results are presented, and in section 8, conclusions are given.

2. Images and segmentation

2.1. Images

The images were obtained from Edinburgh Dermofit Library (https://licensing.edinburgh-innovations.ed.ac.uk/i/software/dermofit-image-library.html). Ballerini L et al., wrote: "The ground truth used for the experiments is based on the agreed classifications by two dermatologists and a pathologist. Images are acquired using a Canon EOS 350D SLR camera. Lighting was controlled using a ring flash, and all images were captured at the same distance (~50 cm), resulting in a pixel resolution of about 0.03 mm" [16]. In this study, images of melanocytic nevus, dermatofibroma, seborrheic keratosis, and melanoma are considered. All photos have the same file type (jpg).

The image bank consists of 729 images divided into four types of skin lesions: 77 of malignant melanoma (MEL), 65 of dermatofibroma (DF), 331 of melanocytic nevus (MN) and 256 of seborrheic keratosis (SK). Where lesions DF, MN, and SK are three types of benign lesions. Figure 1 shows some example images of these lesions. We use these images (DF, MN, and SK) because of look similar to several pictures of melanoma. The conditions for an image to apply this method are: must be in focus and taken normal to the image.

2.2. Segmentation

Segmentation is an essential task in image processing. In the field of the medical image has applications that include, blood cell classification, detection of microcalcifications in mammography, detection of tumors, etc. Different algorithms have been developed to separate an object of interest from the background of an image. One of the most used methods for simplicity is the thresholding, which allows one to segment an image by separating the area of the skin lesion from the background of the picture. The condition to binarize is defined as

$$Mask(x,\ y) = \begin{cases} 1 & if \quad I_{gray}(x,\ y) > T \\ 0 & if \quad I_{gray}(x,\ y) \leq T \end{cases}, \tag{1}$$

where $I_{gray}(x,\ y)$ is the original grayscale image, T is the threshold and $Mask(x,\ y)$ is the resulting mask. Sometimes to get the optimal threshold value, the Otsu method is used. Which considers the maximum variance between classes by an exhaustive search of the background and the skin lesion, defined by

$$T = \max(\sigma^2). \tag{2}$$

Otsu's thresholding is widely used because of its simple calculation. However, in this work to segment the images, a new automated method, called Simple Weighted Otsu Thresholding (SWOT) developed by Zortea *et al.* [17] was used. It is considered that the object of interest

Biomedical Optics EXPRESS

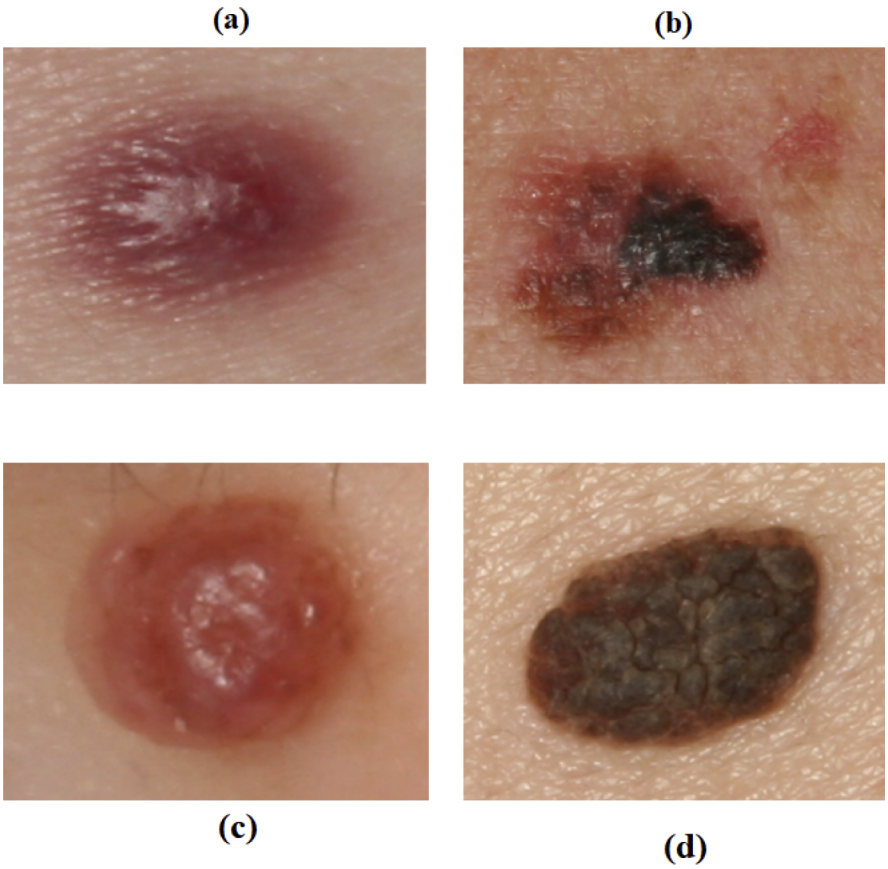

Fig. 1. Skin lesions images. (a) DF. (b) MEL. (c) MN. (d) SK.

is approximately centered on the image, so a transversal diagonal sampling is done. SWOT performs a variation of the Otsu thresholding method, considering the samples in the image and the samples in the cross-diagonals. SWOT is easy to use; the results presented by this method are good.

The images were segmented using the SWOT method to extract only the area that contains skin lesion, generating a binary image, which is called a binary mask. In this way, the healthy skin was removed from each of the images. In this work, with the 98.68% of cases, the segmentation was able to correctly determine the areas of skin lesion and healthy skin.

Once the mask is obtained, a point to point multiplication is performed between the original image and the mask as the final step in the image segmentation. The segmented image is the one used as the input to the system. The process applied to a melanoma image is shown in Fig. 2, where A_{Mask} is the area of the mask over the region of interest, given by:

$$A_{Mask} = \sum_{x,\,y} Mask(x,\ y),\ \text{if}\ Mask(x,\ y) > 0. \tag{3}$$

2.3. Sub-images

In this work, sub-images were used. For obtaining the sub-images, the binary image $Mask(x,\ y)$ corresponding to a specific image is divided into twenty-five sub-masks: $Mask_q(x,\ y)$ for $q = 1, .., 25$. In this way, all images used in this study into 25 sub-images were divided; it is worth

Biomedical Optics EXPRESS

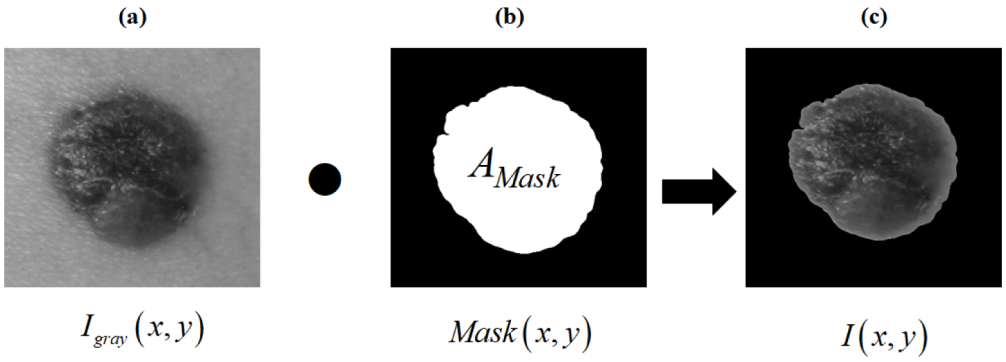

Fig. 2. Segmentation process, where • is a point to point multiplication. (a) Original grayscale image. (b) Mask. (c) Segmented image.

mentioning that these are of different size. Also, the number of sub-images considered for each image depends on the area of the corresponding image. The division process is shown in Fig. 3.

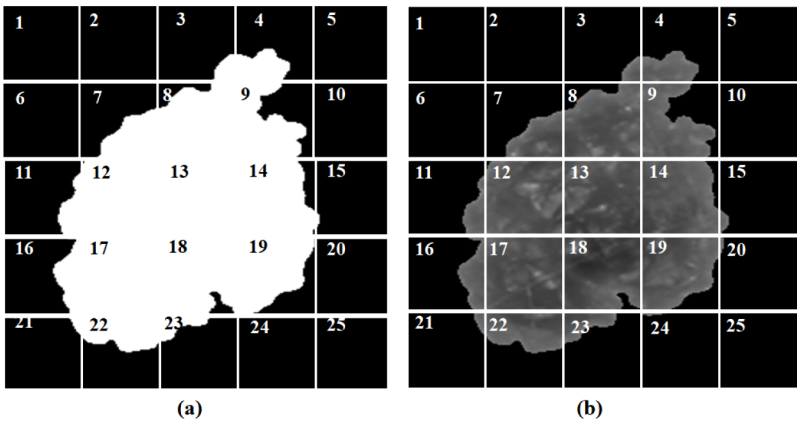

Fig. 3. Image division. (a) Sub-masks $Mask_q(x,\ y)$. (b) Corresponding sub-images $I(x,\ y)_q$.

For this work, only useful sub-images were selected. The selection is made by considering only the sub-images where its corresponding mask has a region of interest with an area:

$$A_{Mask_q} = \sum_{x,\ y} Mask_q(x,\ y),\ \text{if}\ Mask_q(x,\ y) > 0, \tag{4}$$

that complies with the condition:

$$A_{Mask_q} \geq \frac{1}{3}[Area_q], \tag{5}$$

where $Area_q$ is the total area (including the background) of the corresponding sub-mask $Mask_q(x,\ y)$.

In this way, the selected sub-images are the ones that contain information greater or equal to one-third of the total area of the sub-image. Figure 4 shows an example of the sub-images chosen from the image shown in Fig. 3.

Biomedical Optics EXPRESS

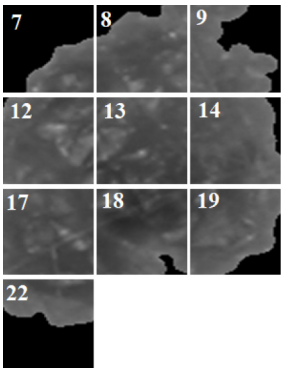

Fig. 4. Sub-images selected for having information greater than or equal to one-third of its area.

3. The fractional Fourier transform

For ease, the 1D definition of the FrFT is presented. The FrFT as defined by Ozaktas *et al.* [18], it can be defined as

$$G_\alpha(u) = \mathcal{F}_\alpha\{g(x)\} = \sqrt{1 - jcot\alpha}\, e^{j\pi u^2 cot\alpha} \int_{-\infty}^{\infty} g(x) e^{j\pi x^2 cot\alpha} e^{-j2\pi u x csc\alpha} dx, \tag{6}$$

where $j = \sqrt{-1}$, x is the variable of the original function in the space domain, u is a dummy variable and α is the rotation angle in the space-frequency plane (Fig. 5). Thus, the FT operator $\mathcal{F}$ to a fractional order p of a function $g(x)$ is $\mathcal{F}^p\{g(x)\} = G^p(u)$, where

$$p = \frac{\alpha}{\pi/2}. \tag{7}$$

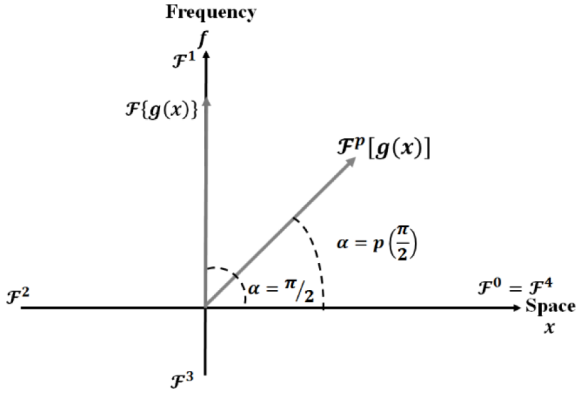

Fig. 5. FrFT representation in the space-frequency plane.

Equation 7 means that by changing the fractional order p, different α angles are achieved, and the classical FT operator is a particular case of the FrFT of order $p = 1$, or equivalently, an angle $\alpha = \pi/2$, as shown in Fig. 5.

Biomedical Optics EXPRESS

4. Fractional nonlinear filter

A nonlinear filter of a function $g(x)$ is defined as

$$NLF\{g(x)\} = |G(u)|^k e^{j\phi(u)}, \tag{8}$$

where $\phi(u)$ is the phase of the Fourier transform and k is the level of nonlinearity [19], which can take values $0 < k < 1$ Eq. (19), and it affects the modulus of the Fourier transform $|G(u)|$.

In this work a nonlinear filter in a fractional plane or fractional nonlinear filter (FrNLF) was used, that is, the modulus of the FrFT of a function $g(x)$ is now affected by the factor k as

$$NLF^p\{g(x)\} = |G^p(u)|^k e^{j\phi(u)}. \tag{9}$$

where p is the order of the FrFT and $k = 0.1$ for this work.

5. The Hermite transform

A polynomial transform is a technique in which signals are locally approximated by polynomials, and the Hermite transform is a particular case that is used to decompose signals and can be regarded as an image description model. The polynomial transform analysis is performed in two steps [20]. In the first step, the image $L(x,\ y)$ is multiplied by a local function or window $v(x-\beta,\ y-\gamma)$. To achieve a complete description of the picture, β and γ are changed to displace the window and create a sampling lattice S. By applying the window along the entire sampling lattice, a weighting function is defined as

$$W(x,\ y) = \sum_{(\beta,\,\gamma)\in S} v(x-\beta,\ y-\gamma), \tag{10}$$

where x and y are the coordinates of a pixel. This weighting function must be different than zero for all coordinates $(x,\ y)$. Therefore,

$$L(x,\ y) = \frac{1}{W(x,\ y)} \sum_{(\beta,\,\gamma)\in S} L(x,\ y)v(x-\beta,\ y-\gamma). \tag{11}$$

As a second step, the local information in each window is expanded in terms of orthogonal Hermite polynomials $G_{\mathrm{M,\ N-}M}(x,\ y)$ that satisfy the orthogonality condition

$$\int_{-\infty}^{\infty}\int_{-\infty}^{\infty} v^2(x,\ y)G_{\mathrm{M,\ N-}M}(x,\ y)G_{\mathrm{L,\ K-}L}(x,\ y)dxdy = \delta_{NL}\delta_{MK}, \tag{12}$$

where M and $N-M$ are the degrees respect to x and y respectively and δ_{NL} and δ_{MK} are Kronecker delta functions, for $N, K = 0, 1, \ldots, \infty$; $M = 0,\ 1,\ \ldots,\ N$ and $L = 0, 1, \ldots K$.

The Hermite transform is a particular case when the windows used are Gaussian functions [20]. The Gaussian window function is defined as

$$v(x,\ y) = \frac{1}{2\pi\sigma^2}\exp\left[\frac{x^2+y^2}{2\sigma^2}\right], \tag{13}$$

where σ is the standard error and the associated orthogonal polynomials are the Hermite polynomials defined as

$$G_{\mathrm{N-M,}\,M}(x,\ y) = \frac{1}{\sqrt{2^N(N-M)!\mathrm{M}!}} H_M\left(\frac{x}{\sigma}\right) H_{N-M}\left(\frac{y}{\sigma}\right), \tag{14}$$

where $H_N(x)$ denotes the Nth Hermite polynomial. Thus Eq. (10) indicates that in every window function, the image content is described as a weighted sum of polynomials $G_{\mathrm{M,\ N-}M}(x,\ y)$ of the

Biomedical Optics EXPRESS

degree M in x and $N-M$ in y. By convolving the original image $L(x,\ y)$ with a filter function $D_{\mathrm{M,\ N-}M}(x,\ y) = G_{\mathrm{N,\ N-}M}(x,\ y)v^2(-x,\ -y)$, following with a subsampling at the location $(\beta,\ \gamma)$ of S, we get the polynomial coefficients

$$L_{m,\ n-m}(\beta, \gamma) = \int_{-\infty}^{\infty}\int_{-\infty}^{\infty} L(x,\ y)D_{\mathrm{M,\ N-}M}(x-\beta,\ y-\gamma)dxdy. \tag{15}$$

Therefore, for the Hermite transform, the filter functions correspond to Gaussian derivates of order M in x and $N-M$ in y [21].

Figure 6 shows an example of the Hermite transform of an image of a melanoma lesion, considering the transform order.

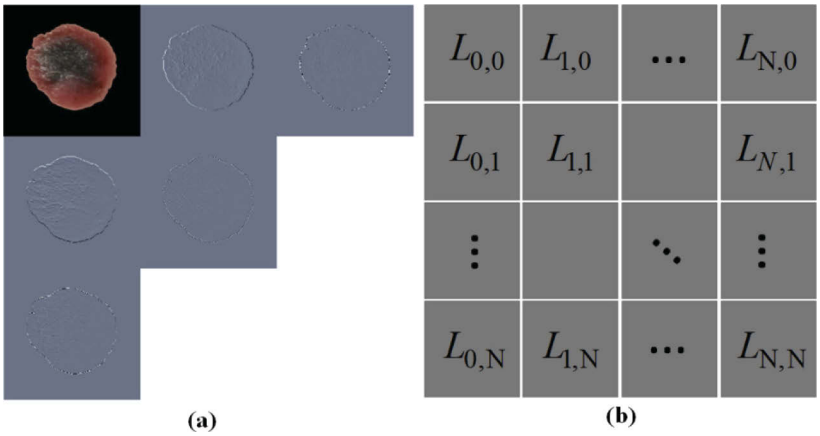

Fig. 6. (a) Hermite transform of melanoma image. (b) Diagram of coefficient orders.

In recent work, Castro-Valdez and Álvarez-Borrego [22], used the Hermite transform joint to classical correlation to recognize phytoplankton species and based on the noise in the output correlation plane, demonstrated that the optimal order of the Hermite transform is $L_{1,1}$.

6. Spectral indexes

6.1. Spectral indexes of an image using the FrNLF of the selected sub-images

For this task, first, the FrNLF of a selected sub-image is obtained. Next, the binary fractional spectral densities (*SSFR*) are calculated by applying the conditions

$$\begin{aligned}
SSFR_{1_q} &= \left\{ \begin{array}{l} 1, \text{ if } \mathrm{Re}[NLF^p\{I_q(x,\ y)\}] \geq 0 \\ 0, \text{ otherwise} \end{array} \right\}, \\
SSFR_{2_q} &= \left\{ \begin{array}{l} 1, \text{ if } \mathrm{Re}[NLF^p\{I_q(x,\ y)\}] < 0 \\ 0, \text{ otherwise} \end{array} \right\}, \\
SSFR_{3_q} &= \left\{ \begin{array}{l} 1, \text{ if } \mathrm{Im}[NLF^p\{I_q(x,\ y)\}] \geq 0 \\ 0, \text{ otherwise} \end{array} \right\}, \\
SSFR_{4_q} &= \left\{ \begin{array}{l} 1, \text{ if } \mathrm{Im}[NLF^p\{I_q(x,\ y)\}] < 0 \\ 0, \text{ otherwise} \end{array} \right\},
\end{aligned} \tag{16}$$

Biomedical Optics EXPRESS

where $\mathrm{Re}[NLF^p\{I_q(x,\ y)\}]$ and $\mathrm{Im}[NLF^p\{I_q(x,\ y)\}]$ are the real and imaginary parts respectively of the FrNLF of the sub-image, q is the number of the sub-image and p is the fractional order. Thus the fractional spectral indexes of each sub-image are

$$index_{n_q}^{SSFR} = \frac{A_{Mask_q}}{SSFR_{n_q}}, \tag{17}$$

where $n = 1, 2, 3, 4$ and A_{Mask_q} is the sum of the unit values present in the sub-image mask.

Finally, the fractional spectral indexes for the corresponding image are obtained as

$$\overline{index_n^{SSFR}} = \frac{\sum_{1}^{Q} index_{n_q}^{SSFR}}{Q}, \tag{18}$$

where $n = 1, 2, 3, 4$ and Q is the total number of sub-images extracted from the image, which agree with the condition of Eq. (5).

6.2. Spectral index using the FrFT of the Hermite transform (HT)

A variation of the method described in section 6.1, it is when the indexes are obtained by calculating the Hermite transform of the order $(1, 1)$ of a sub-image before calculating its fractional nonlinear filter and extract its real and imaginary parts to apply the four conditions in Eq. (16) to obtain the binary fractional spectral density.

7. Computer analysis

7.1. Optimal order of the FrFT

From section 3, it can be observed that the fraction order p can take values between 0 to 1, which select points between the space domain and the frequency domain; therefore, an optimal order p must be selected. For the search of the optimal order for each of the four spectral indexes, the 76 images of melanoma (MEL) are used as a reference. Then, for the selected sub-images of each melanoma image, the fractional spectral indexes are obtained for a particular order p, and the mean of the fractional spectral indexes are calculated based on the results in Eq. (16), as

$$mean(\overline{index_n^{SSFR}}) = \frac{\sum_{m=1}^{76} \overline{index_{n_m}^{SSFR}}}{76}, \tag{19}$$

where m is the number of the melanoma image processed. The process is repeated by changing the order p from 0.01 to 1, in steps of 0.01, and the order that gives us the higher mean value is the optimal order for the respective fractional spectral index. The optimum orders for each fractional spectral index for sub-images are shown in Table 1.

Table 1. Optimum orders for each fractional spectral index using sub-images.

Index	Order p
$\overline{index_1^{SSFR}}$	0.9
$\overline{index_2^{SSFR}}$	0.01
$\overline{index_3^{SSFR}}$	0.03
$\overline{index_4^{SSFR}}$	0.91

For the case when the HT is used, the optimum orders are obtained the same way. Table 2 shows the optimum orders for the method when the HT of the sub-images are calculated.

Biomedical Optics EXPRESS

Table 2. Optimum orders for each fractional spectral index using the HT of the sub-images.

Index	Order p
$index_1^{SSFR}$	1
$index_2^{SSFR}$	0.01
$index_3^{SSFR}$	0.01
$index_4^{SSFR}$	0.53

7.2. Results of the discrimination process applied to all four types of skin lesions

The method described in section 6.1, was repeated with the images of each skin lesion, and an interval of the mean indexes ±3 standard errors (Table 3), which gives a 99.7% confidence level was generated. This process was done using the optimum orders shown in Table 1. The same interval was obtained for the variation described in section 6.2 when the HT is implemented, using the optimum orders shown in Table 2 (Table 4).

Table 3. Fractional spectral indexes intervals for melanoma images.

Index	Intervals for *malignant melanoma*
$index_1^{SSFR}$	114.2 - 142.4
$index_2^{SSFR}$	130.3 - 171
$index_3^{SSFR}$	123.2 - 156.6
$index_4^{SSFR}$	114.3 - 142.6

Table 4. Fractional spectral indexes Intervals for the melanoma images implementing the Hermite transform.

Index	Intervals for *malignant melanoma*
$index_1^{SSFR}$	139.6 - 187.6
$index_2^{SSFR}$	109.7 - 137.4
$index_3^{SSFR}$	109.3 - 136.4

The diagnosis of a skin lesion by a dermatologist remains subjective. The diagnostic accuracy range is 64% to 80% [23–26], measured in specialized dermatology centers. Nowadays, most diagnoses are made by physician assistants, which accuracy is lower than the dermatologists [27].

Because the images of melanoma (MEL) were used as a reference, then, by working with these optimum orders, better discrimination between melanoma and the other skin lesions is expected. The results when the FrNLF of the sub-images is used are sown in Fig. 7, showing box-whisker plot with median, quartiles and outliers of box plot.

There is an overlap, for the four cases on 25%-75% quartiles; however, the median value is lower in all the instances for MEL. These graphs show results more transparent. Sensitivity and specificity were calculated (Table 5). Bad results can be seen in all cases. Sensitivity values are so low for melanoma, and most of the cases, specificity is less than 80%. For this reason, to use fractional Fourier transform with a mean spectral index does not work.

For the case when the FrNLF of the HT of the sub-images is implemented, the results are shown in Fig. 8. In this case, there is not an overlap of melanoma on 25%-75% quartiles for case (a). Analyzing the values obtained for sensitivity and specificity (Table 6), we can see that, case (a) is the only way to determine melanoma with a precision better than dermatologists [23–26].

However, in this case is used the order 1 (Table 2), in another words, the classical Fourier transform is used. For this reason, talking about the mean of the spectral index, the interval used for melanoma detection is 139.6-187.6.

Biomedical Optics EXPRESS

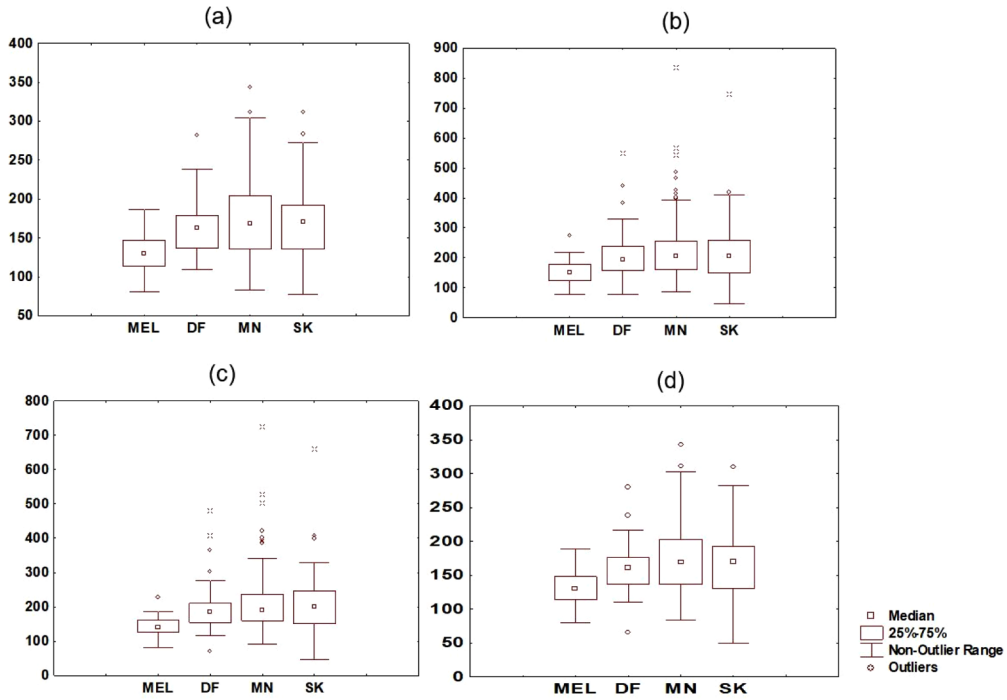

Fig. 7. Results of the fractional spectral indexes of sub-images. (a) $\overline{index_1^{SSFR}}$. (b) $\overline{index_2^{SSFR}}$. (c) $\overline{index_3^{SSFR}}$. (d) $\overline{index_4^{SSFR}}$.

Table 5. Sensitivity and Specificity for FrNLF

Sensitivity – Index 1	ML= 43.24 %
Specificity – Index 1	DF = 80.77 %
Specificity – Index 1	MN = 78.82 %
Specificity – Index 1	SK = 78.37 %

Sensitivity – Index 2	ML= 40.54 %
Specificity – Index 2	DF = 75.00 %
Specificity – Index 2	MN = 80.55 %
Specificity – Index 2	SK = 76.75 %

Sensitivity – Index 3	ML= 43.24 %
Specificity – Index 3	DF = 76.92 %
Specificity – Index 3	MN = 84.37 %
Specificity – Index 3	SK = 81.08 %

Sensitivity – Index 4	ML= 43.24 %
Specificity – Index 4	DF = 76.92 %
Specificity – Index 4	MN = 77.77 %
Specificity – Index 4	SK = 77.83 %

Biomedical Optics EXPRESS

Table 6. Sensitivity and Specificity for FrNLF with Hermite

Sensitivity – Index 1	ML= 89.18%
Specificity – Index 1	DF = 82.69 %
Specificity – Index 1	MN = 86.45 %
Specificity – Index 1	SK = 88.10 %

Sensitivity – Index 2	ML= 60.04 %
Specificity – Index 2	DF = 80.76 %
Specificity – Index 2	MN = 79.16 %
Specificity – Index 2	SK = 79.46 %

Sensitivity – Index 3	ML= 61.03 %
Specificity – Index 3	DF = 82.69 %
Specificity – Index 3	MN = 78.13 %
Specificity – Index 3	SK = 76.75 %

Sensitivity – Index 4	ML= 53.24 %
Specificity – Index 4	DF = 73.07 %
Specificity – Index 4	MN = 76.04 %
Specificity – Index 4	SK = 78.91 %

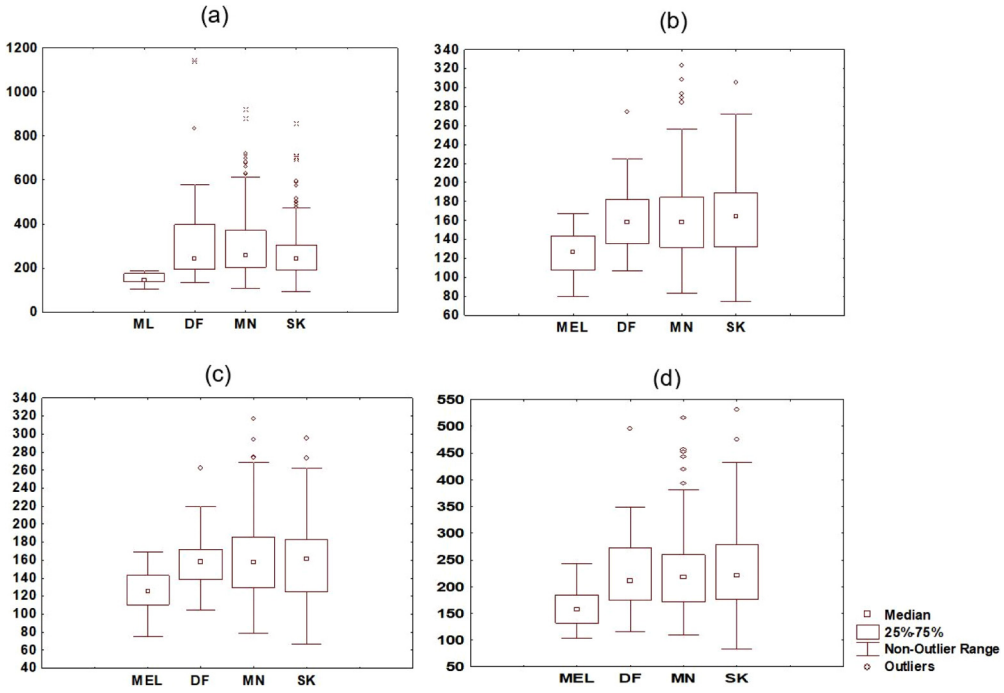

Fig. 8. Results of the fractional spectral indexes when working with the HT of sub-images. (a) $\overline{index_1^{SSFR}}$. (b) $\overline{index_2^{SSFR}}$. (c) $\overline{index_3^{SSFR}}$. (d) $\overline{index_4^{SSFR}}$.

Biomedical Optics EXPRESS

The time consumption was 2 s for the first method and 2.2 s when HT is used. The times were obtained in a Windows 10 computer with a 3.40 GHz Intel Core i7-3770 and 8 GB DDR3 RAM.

8. Conclusions

This paper presents a new methodology for the discrimination of malignant melanoma skin cancer from other three types of benign skin lesions based on fractional spectral indexes obtained in two ways, first, when only the fractional Fourier transform is used to generate the nonlinear filter. Second, when the Hermite transform is used before the fractional Fourier transform is applied. Both approaches were employed when sub-images are extracted from an image.

Box-whisker plot with median, quartiles and outliers of box plot were used in these analysis. For the case when the FrNLF of the HT of the sub-images is implemented, there is not an overlap of melanoma on 25%-75% quartiles for case (a). This is the only way to determine melanoma with a precision better than dermatologists. For this reason, talking about the mean of the spectral index, the interval used for melanoma detection is 139.6-187.6.

Acknowledgments

Esbanyely Garza-Flores was a student in the PhD program of Optics Department in CICESE and supported by CONACyT's scholarship.

Disclosures

The authors declare that there are no conflicts of interest related to this article.

References

1. A. Taloni, A. A. Alemi, E. Ciusani, J. P. Sethna, S. Zapperi, and C. A. M. La Porta, "Mechanical properties of growing melanocytic nevi and the progression to melanoma," PLoS One **9**(4), e94229 (2014).
2. L. Parish, S. Yazdanian, W. C. Lambert, and P. C. Lambert, "Dermatofibroma: a curious tumor," Thomas Jefferson Univ. Jefferson Digit Commons Dep. **10**(5), 268–270 (2012).
3. J. Q. Del Rosso, "A Closer Look at Seborrheic Keratoses: Patient Perspectives, Clinical Relevance, Medical Necessity, and Implications for Management," J. Clin. Aesthet. Dermatol. **10**(3), 16–25 (2017).
4. American Cancer Society. Cancer Facts & Figures. 2014.
5. S. Ogden and N. R. Telfer, "Skin cancer," Medicine **37**(6), 305–308 (2009).
6. M. Helfand, S. Mahon, and K. Eden, "Screening for skin cancer," Am. J. Prev. Med. **20**(3), 47–58 (2001).
7. T. Y. Tan, L. Zhang, and M. Jiang, "An intelligent decision support system for skin cancer detection from dermoscopic images," *12th Int Conf Nat Comput Fuzzy Syst Knowl Discov.* (2016).
8. N. C. F. Codella, D. Gutman, M. E. Celebi, B. Helba, M. A. Marchetti, S. W. Dusza, A. Kalloo, K. Liopyris, N. Mishra, H. Kittler, and A. Halpern, "Skin lesion analysis toward melanoma detection: A challenge at the 2017 International symposium on biomedical imaging (ISBI), hosted by the international skin imaging collaboration (ISIC)," *Proc. - Int. Symp. Biomed. Imaging.* (2018).
9. K. Korotkov and R. Garcia, "Computerized analysis of pigmented skin lesions: a review," Artif. Intell. Med. **56**(2), 69–90 (2012).
10. A. G. Isai, B. G. Zapirain, and A. M. Zorrilla, "Melanomas non-invasive diagnosis application based on the ABCD rule and pattern recognition image processing algorithms," Comput. Biol. Med. **41**(9), 742–755 (2011).
11. M. M. Rahman and P. Bhattacharya, "An integrated and interactive decision support system for automated melanoma recognition of dermoscopic images," Comput. Med. Imaging Graph. **34**(6), 479–486 (2010).
12. J. A. Jaleel, S. Salim, and R. B. Aswin, "Artificial neural network based detection of skin cancer," IJAREEIE. **1**, 200–2005 (2012).
13. G. Betta, G. Di Leo, G. Fabbrocini, A. Paolillo, and P. Sommella, "Dermoscopic image-analysis system: estimation of atypical pigment network and atypical vascular pattern," presented at the *International Workshop on Medical Measuremet and Applications*, Beneto, Italy, 20-21 Abril 2006.
14. E. Guerra-Rosas and J. Alvarez-Borrego, "Methodology for diagnosis of skin cancer on images of dermatologic spots by spectral analysis," Biomed. Opt. Express **6**(10), 3876–3891 (2015).
15. E. Guerra-Rosas, J. Álvarez-Borrego, and A. Angulo-Molina, "Identification of melanoma cells: a method based in mean variance of signatures via spectral densities," Biomed. Opt. Express **8**(4), 2185–2194 (2017).
16. L. Ballerini, R. B. Fisher, R. B. Aldridge, and J. Rees, "A Color and Texture Based Hierarchical K-NN Approach to the Classification of Non-melanoma Skin Lesions," in M. E. Celebi and G. Schaefer (eds.), *Color Medical Image*

Biomedical Optics EXPRESS

Analysis, Lecture Notes in Computational Vision and Biomechanics 6, ISBN 978-94-007-5389-1, (Springer, 2013), 1–26.
17. M. Zortea, E. Flores, and J. Scharcanski, "A simple weighted thresholding method for the segmentation of pigmented skin lesions in macroscopic images," Pattern Recognit. **64**, 92–104 (2017).
18. H. M. Ozaktas, M. A. Kutay, and D. Mendlovic, "Introduction to the Fractional Fourier Transform and its Applications," Adv. Imag. Electron. Phys. **106**, 239–291 (1999).
19. B. Javidi, W. Wang, and G. Zhang, "Composite Fourier-plane nonlinear filter for distortion-invariant pattern recognition," Opt. Eng. **36**(10), 2690–2696 (1997).
20. M. Jean-Bernard, "The Hermite Transform-Theory," IEEE Trans. Acoust., Speech, Signal Process. **38**(9), 1595–1606 (1990).
21. B. Escalante-Ramírez, "The Hermite transform as an efficient model for local image analysis: An application to medical image fusion," Comput. Electr. Eng. **34**(2), 99–110 (2008).
22. A. Castro-Valdez and J. Álvarez-Borrego, "Identification of phytoplankton species using Hermite transform," Ukr. J. Phys. Opt. **19**(2), 106–120 (2018).
23. A. R. MacKenzie-Wood, G. W. Milton, and J. W. Launey, "Melanoma: Accuracy of clinical diagnosis," Australas. J. Dermatol. **39**(1), 31–33 (1998).
24. M. Miller and A. B. Ackerman, "How accurate are dermatologists in the diagnosis of melanoma? degree of accuracy and implications," Arch. Dermatol. **128**(4), 559–560 (1992).
25. B. Lindel and M. A. Hedblad, "Accuracy in the clinical diagnosis and pattern of malignant melanoma at a dermatological clinic," J. Dermatol. **21**(7), 461–464 (1994).
26. C. M. Grin, A. W. Kopf, B. Welkovich, R. S. Bart, and M. J. Levenstein, "Accuracy in the clinical diagnosis of malignant melanoma," Arch. Dermatol. **126**(6), 763–766 (1990).
27. A. M. Anderson, M. Matsumoto, M. I. Saul, A. M. Secrest, and L. K. Ferris, "Accuracy of skin cancer diagnosis by physician assistants compared with dermatologists in a large health care system," JAMA Dermatol. **154**(5), 569–573 (2018).